Geochimica et Cosmochimica Acta, Vol. 69, No. 9, pp. 2361–2371, 2005

0016-7037/05 $30.00 + .00

doi:10.1016/j.gca.2004.11.015

Partitioning of trace elements between rutile and silicate melts: Implications for subduction zones

Stephan Klemme,[1,*] Stefan Prowatke,[1] Kathrin Hametner,[2] and Detlef Günther[2]

[1]Mineralogisches Institut, Universität Heidelberg, Im Neuenheimer Feld 236, 69120 Heidelberg, Germany
[2]Laboratorium für Anorganische Chemie, Eidgenössische Technische Hochschule Zürich, ETH Hönggerberg, 8093 Zürich, Switzerland

(*Received April* 26, 2004; *accepted in revised form November* 17, 2004)

Abstract—Mineral/melt trace element partition coefficients were determined for rutile (TiO_2) for a large number of trace elements (Zr, Hf, Nb, Ta, V, Co, Cu, Zn, Sr, REE, Cr, Sb, W, U, Th). Whilst the high field strength elements (Zr, Hf, Nb, Ta) are compatible in rutile, other studied trace elements are incompatible (Sr, Th, REE). In all experiments we found $D_{Ta} > D_{Nb}$, $D_{Hf} > D_{Zr}$ and $D_U > D_{Th}$. Partition coefficients for some polyvalent elements (Sb, W, and Co) were sensitive to oxygen fugacity. Melt composition exerts a strong influence on HFSE partition coefficients. With increasing polymerization of the melt, rutile/melt partition coefficients for the high field strength elements Zr, Hf, Nb and Ta increase about an order of magnitude. However, D_{Nb}/D_{Ta} and D_{Hf}/D_{Zr} are not significantly affected by melt composition. Because $D_U \gg D_{Th}$, partial melting of rutile-bearing eclogite in subducted lithosphere may cause excesses of ^{230}Th over ^{238}U in some island arc lavas, whereas dehydration of subducted lithosphere may cause excesses of ^{238}U over ^{230}Th. From our partitioning results we infer partition coefficients for protactinium (Pa) which we predict to be much lower than previously anticipated. Contrary to previous studies, our data imply that rutile should not significantly influence observed ^{231}Pa-^{235}U disequilibria in certain volcanic rocks. *Copyright © 2005 Elsevier Ltd*

1. INTRODUCTION

Understanding magmatic processes at convergent plate boundaries is essential for understanding mass transfer between geochemical reservoirs of the Earth and the origin and growth of continents. The subducting oceanic crusts undergoes a number of metamorphic changes that are accompanied by the release of fluids during progressive dehydration. It is thought that released fluids metasomatize the overlying mantle wedge and induce melting in the mantle which, ultimately, leads to magmatism in island arcs (e.g., Tatsumi and Eggins, 1995; Ayers, 1998). Most thermal models for subduction zones indicate that the subducted crust dehydrates, but remains below its solidus (Peacock, 1991; Davies and Stevenson, 1992; Peacock, 1996). More recent thermal models have challenged this view suggesting that melting of relatively old crust may indeed be possible (Kelemen et al., 2004). If correct, this implies that partial melting of the subducted crust in normal subduction zones may be a much more common process than has been previously accepted. Certainly, however, in extraordinary subduction settings with young and hot oceanic crust, subducted basalt may melt and produce calc-alkaline magmas, the so-called adakites (e.g., Defant and Drummond, 1990). Adakites are characterized by enrichment in silica, sodium, Sr and La (and light rare earth elements), with low Y and steep rare earth element (REE) patterns (e.g., Defant and Drummond, 1990; Stern and Kilian, 1996). Moreover, adakites, as most other volcanic arc rocks, are characterized by very low concentrations of high field strength elements (HFSEs). Archaean tonalites, trondhjemites, and granodiorites (TTG) have similar chemical compositions (e.g., Martin, 1987; Defant and Drummond, 1990; Drummond and Defant, 1990; Stern and Kilian, 1996; Yogodzinski and Kelemen, 1998; Leybourne et al., 1999) and are also interpreted to be products of partial melting of the subducted slab (Drummond and Defant, 1990; Leybourne et al., 1999; Barth et al., 2002; Foley et al., 2002; Klemme et al., 2002; Rapp et al., 2003).

As rutile (TiO_2) is known to incorporate significant amounts of the HFSEs (Green and Pearson, 1987; Zack et al., 2002) many models suggest that rutile is the mineral that retains the HFSEs during slab devolatization or melting, whereas other incompatible elements are partitioned into the melt or fluid. Despite its important role in subduction zone processes, there is scant experimental data on how trace elements partition between silicate magmas and rutile crystals (McCallum and Charette, 1978; Green and Pearson, 1987; Jenner et al., 1993; Foley et al., 2000; Green, 2000; Horng and Hess, 2000; Schmidt et al., 2004). Experimental studies on the partitioning of trace elements between rutile and silcate melts have focussed on the high field strength elements. Several previous studies have shown that Nb and Ta are strongly compatible in rutile (Fig. 1) with the absolute values of the partition coefficients between 2 and more than 100, and most partitioning studies (Table 1) agree that rutile/melt $D_{Ta} > D_{Nb,}$ only Linnen and Keppler (1997) predicted $D_{Nb} > D_{Ta}$ based on columbite solubility in granitic melts. A recent study investigated the partitioning of a large number of trace elements between rutile and melt (Foley et al., 2000). They also report values for D_{Hf} and D_{Zr} which they found slightly compatible and partition coefficients for several other trace elements (REE, Sr, Ba, Rb) that were, as one might expect from crystal chemical considerations, incompatible in rutile (Foley et al., 2000). Another recent study investigated the partitioning Nb and Ta between rutile and granitic melts of very different compositions (Horng and Hess, 2000). They proposed a significant effect of the melt

* Author to whom correspondence should be addressed (sklemme@min.uni-heidelberg.de).

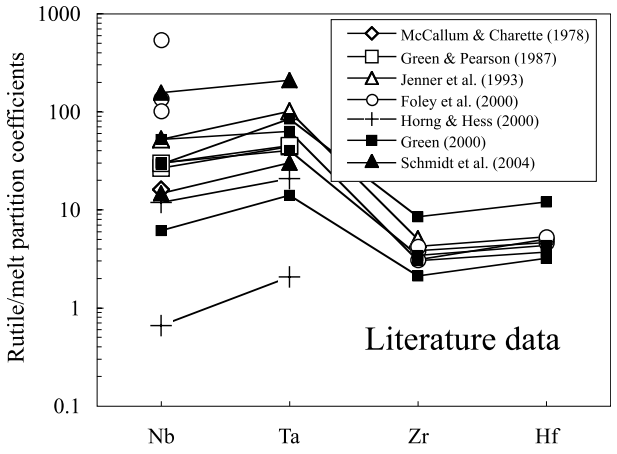

Fig. 1. Previous rutile/melt partition coefficients taken from the literature. Note also that Horng and Hess (2000) investigated rutile partition coefficients for Nb and Ta in haplogranitic compositions to investigate the effect of melt composition on partition coefficients. For clarity, only maximum and minimum values of D_{Nb} and D_{Ta} (Horng and Hess, 2000) are shown here. Note that D_{Nb} ranges from incompatible ($D_{Nb} < 1$) to very compatible $D_{Nb} \gg 1$, whereas D_{Ta} is always compatible.

composition on partition coefficients. Figure 1 and Table 1 give a summary of previous data on rutile/melt partitioning. As there is a considerable spread of Nb and Ta partition coefficients and relatively limited data on Zr, Hf, and other trace elements we initiated a systematic study aimed at a better understanding of rutile/melt partitioning.

Two main sets of experiments were performed: First, we conducted a series of partitioning experiments in synthetic andesitic and rhyolitic bulk compositions. These experiments were performed at identical temperature and pressure but with varying oxygen fugacities (fO_2) to investigate a possible effect of fO_2 on the partitioning of polyvalent elements. Note that experiments in basaltic compositions always yielded pseudobrookite, Fe-Ti spinels, or ilmenite.

In this context, it should be mentioned that the partitioning of trace elements between crystals and melts is a complex function of several parameters, such as pressure, temperature, oxygen fugacity, crystal composition, and melt composition (e.g., Watson, 1976; Ryerson and Hess, 1978; Blundy and Wood, 1994; Green, 1994; Kohn and Schofield, 1994; Horng and Hess, 2000; Klemme et al., 2002; Klemme and Dalpé, 2003). As a number of papers have identified melt composition as a significant factor (Watson, 1976; Ryerson and Hess, 1978; Lesher, 1986; Nielsen et al., 1992; Kohn and Schofield, 1994; Linnen and Keppler, 1997, 2002; Horng and Hess, 2000; Kushiro and Mysen, 2002; O'Neill and Eggins, 2002; Klemme and Dalpé, 2003; Klemme and Meyer, 2003; Prowatke and Klemme, 2005; Schmidt et al., 2004), we designed four additional experiments along a compositional vector that allowed us to study the effect of melt composition on the partitioning. As the major element composition of rutile is virtually constant in the experiments, we can exclude a significant role of the mineral composition on trace element partition coefficients and examine the effect of melt composition on the partitioning of trace elements.

2. EXPERIMENTS

2.1. Starting Materials

Two starting material mixtures were prepared that were similar to andesitic compositions (SKHDAN1) and rhyolitic compositions (SKHDRH1), respectively (Table 2). Starting major element compositions were prepared by mixing together the appropriate amounts of reagent grade oxides and carbonates (MgO, Fe_2O_3, $CaCO_3$, Na_2CO_3, K_2CO_3, Al_2O_3 and SiO_2). MgO and Al_2O_3 were initially fired at 1050°C to drive off any residual moisture. All starting materials were stored at 110°C. Subsequently, a trace element cocktail consisting of pure oxides and carbonates of 21 trace elements (Table 2) was added. The starting material mixtures were then ground under acetone in an agate mortar to produce homogeneous mixtures. These mixtures were decarbonated at 1000°C for 4 h, melted at 1400°C and subsequently at 1600°C, and then quenched to a glass. This procedure was repeated three times, with fine grinding in between. ~30 mol% ultrapure TiO_2 was added to these compositions. The resulting mixtures were mixed again, melted in a Platinum crucible at 1500°C and subsequently quenched to a glass. Furthermore, four additional bulk compositions were prepared with varying alumina saturation index (ASI: molar ratio $Al_2O_3/(Na_2O + K_2O + CaO)$). These starting materials were prepared in a similar way as the synthetic rock compositions. The major and trace element compositions of the starting materials are given in Table 2.

Table 1. Literature experimental rutile/melt partition coefficients.[a]

	D_{Nb}	D_{Ta}	D_{Zr}	D_{Hf}	Melt composition	P (GPa)	T (°C)
McCallum and Charette (1978)	16		—	—	basalt	1 atm	1105
Green and Pearson (1987)	26.5	44	—	—	andesite	1.6	1000
Green and Pearson (1987)	29.8	44.7	—	—	trachyte	0.4	1000
Jenner et al. (1993)	52.6	99.5	4.8		tonalite	3.5	1000
Foley et al. (2000)	540	—	3.8	4.6	tonalite	1.8	900
Foley et al. (2000)	136	—	3.1	5	tonalite	1.8	1025
Foley et al. (2000)	102	—	4.2	5.3	tonalite	2.5	1100
Green (2000)	6.1	14	2.1	3.2	basalt	3–3.5	1100
Green (2000)	30	40	3.4	4.3	andesite	3–3.5	1000
Green (2000)	52	63	3	3.7	rhyodacite	3–3.5	1000
Green (2000)	29	84	8.5	12	carbonatite	2.5	1000
Schmidt et al. (2004)	15–156	30–209	—	—	basalt-rhyolite	1.7–2.5	950–1300
Horng and Hess (2000)	0.7–11.8	2–21	—	—	haplogranite	1 atm	1400

[a] P = pressure (GPa), T = temperature (°C). D = c mineral/c melt. Note that Foley et al. (2000) only place upper bounds on D_{Ta} and are therefore not given here. Note that Horng and Hess (2000) and Schmidt et al. (2004) investigated the influence of melt composition on the partitioning of Nb and Ta. Given here are only selected results from their experiments that contained both Nb and Ta. Refer to Horng and Hess (2000) for further details.

Table 2. Major element (wt%) and trace element composition of starting materials [ppm] and experimental run conditions.[a]

	SKHDAN1	SKHDRH1	SMNa	SM20	SM40	SM40H
SiO_2	45.8	56.0	39.2	40.4	41.7	41.7
TiO_2	23.7	20.0	36.0	32.4	28.8	28.8
Al_2O_3	15.3	12.0	3.1	7.6	12.0	12.0
Na_2O	6.1	6.4	11.8	9.8	7.8	7.8
K_2O	3.1	5.6	1.9	1.5	1.1	1.1
CaO	6.1	b.d.	2.3	2.3	2.4	2.4
MgO	b.d.	b.d.	1.8	1.9	1.9	1.9
FeO	b.d.	b.d.	4.0	4.1	4.3	4.3
La	442 (14)	1.7 (4)				
Ce	1255 (39)	1321 (98)				
Pr	646 (28)	0.4 (1)				
Sm	385 (22)	546 (4)				
Gd	1356 (38)	0.27 (11)				
Lu	690 (40)	0.14 (5)				
Co	533 (17)	0.5 (1)				
Cu	153 (10)	4.4 (3)				
Zn	24 (2)	32 (7)				
Sr	438 (18)	283 (24)	73 (2)	71 (2)	68 (2)	68 (2)
V	139 (13)	147 (27)	64 (2)	68 (3)	71 (2)	71 (2)
Cr	401 (32)	5.6 (38)				
W	2012 (78)	257 (43)	48 (3)	52 (3)	56 (3)	56 (3)
Sb	432 (11)	110 (19)	538 (10)	614 (19)	695 (39)	695 (39)
Zr	1280 (159)	166 (36)	76 (1)	78 (1)	79.9 (13)	79.9 (13)
Hf	756 (73)	306 (121)	66 (2)	67.8 (25)	69.3 (28)	69.3 (28)
Nb	571 (105)	1033 (155)	274 (6)	288 (7)	302 (8)	302 (8)
Ta	1312 (147)	816 (220)	201 (16)	216 (16)	231 (16)	231 (16)
Th	1359 (53)	103 (20)	61 (3)	62 (3)	62 (4)	62 (4)
U	395 (16)	1048 (275)	79 (3)	81 (1)	82 (5)	82 (5)
Pb	1774 (70)	344 (60)				

Experimental run conditions

Run No.	Starting material	Redox conditions (log fO_2)	T °[C]	Phases Present	Run duration (h)
MHD15_1	SKHDAN1	−0.96	1250	TiO_2, glass	57
HD4_4	SKHDAN1	−4.0	1250	TiO_2, glass	49
HD2_4	SKHDAN1	−11.3	1250	TiO_2, glass	72
MHD16_1	SKHDRH1	−4.0	1250	TiO_2, glass	51
RT10-Na	SMNa	−3.3	1300	TiO_2, glass	60
RT10–20	SM20	−3.3	1300	TiO_2, glass	60
RT10–40	SM40	−3.3	1300	TiO_2, glass	60
RT10–40H	SM40H	−3.3	1300	TiO_2, glass	60

[a] Major element concentrations of starting materials were analysed with the electron microprobe (w. %, normalized to 100%). Note that trace elements of starting material glasses SKHDAN1 and SKHDRH1 were analyzed with laser ablation ICPMS, whereas the other trace element concentrations were analyzed using SIMS (ppm). Uncertainties given as last significant digits (1 σ). The MHD and HD runs were initially heated to 1430°C and then slowly cooled (5°C/h) to the final run temperature of 1250°C. The RT runs were first heated to 1483°C, and then slowly cooled (5°C/h) to 1300°C. fO_2 = oxygen fugacity (Deines et al., 1974). Run duration = run duration at final temperature, given in hours. b.d. = below detection.

Although the experiments are unreversed (as in most other trace element partitioning studies and melting equilibria studies), there is evidence that equilibrium was attained in our experiments as mineral and glass analyses have low standard deviations indicating homogenous, unzoned phase compositions (Table 2). Moreover, as the analytical results (Table 3) indicate, there is excellent agreement between partition coefficients from experiments where trace elements were added in very different concentrations. This supports the attainment of equilibrium between crystals and melts and also indicates Henry's law behavior in our experiments.

2.2. Experimental and Analytical Techniques

High-temperature experiments were conducted at atmospheric pressure in conventional vertical quench furnaces at atmospheric pressure. Oxygen fugacity in the furnace was controlled by varying proportions of CO and CO_2 in the furnace using Tylan digital gas flow controllers. Temperatures were measured before and after the runs with a type S (Pt-$Pt_{90}Rh_{10}$) thermocouple, which was previously calibrated against the melting points of gold (1064.4°C) and nickel (1455.0°C) (Dinsdale, 1991). The temperature was controlled within 0.2°C using Eurotherm controllers. All experiments were initially heated above their liquidus and subsequently cooled at constant rates of 5°C per hour to 1250°C or 1300°C (Table 2). These particular temperatures were chosen because no other phases were found to exist next to rutile and the melt fraction in the experimental run products is usually much greater than 50%. Samples were held at the final run temperature for a duration of up to 60 h to allow equilibration of rutile and coexisting melts (see Table 2 for details). All experiments were terminated by quenching the samples into double-distilled water. Using the so-called wire-loop-technique (Corrigan and Gibb, 1979; Donaldson and Gibb, 1979) it was possible to run several samples simultaneously. Moreover, the use of thin

Table 3. Major and trace element compositions of experimental run products and partition coefficients.[a]

Major elements rutiles (wt%)

Run	MHD15_1	HD4_4	HD2_4	MHD16_1	RT10-Na	RT10–20	RT10–40	RT10–40H
Al_2O_3	0.15 (8)	0.15 (6)	0.16 (4)	0.11 (5)	n.d.	0.05 (10)	0.20 (3)	0.24 (2)
TiO_2	99.9 (1)	99.9 (1)	99.9 (2)	99.9 (1)	100 (1)	100 (1)	99.4 (3)	99.6 (3)
FeO	b.d.	b.d.	0.1 (1)	b.d.	b.d.	0.57	0.9 (1)	0.9 (1)
total	100.1	100.1	100.2	100.0	100.3	100.7	100.5	100.8

Major element melts (wt%)

Run	MHD15_1	HD4_4	HD2_4	MHD16_1	RT10-Na	RT10–20	RT10–40	RT10–40H
Na_2O	2.4 (1)	2.2 (1)	1.6 (2)	1.7 (1)	>10.5 (1)	>9.8 (2)	8.6 (2)	7.5 (2)
MgO	b.d.	b.d.	>0.1 (1)	b.d.	2.0 (1)	2.1 (1)	2.3 (1)	2.4 (1)
Al_2O_3	17.3 (1)	18.1 (1)	19.3 (2)	13.2 (1)	3.4 (1)	>8.0 (1)	13.8 (2)	14.5 (2)
SiO_2	>57.7 (3)	59.0 (3)	>61.2 (4)	74.6 (5)	43.3 (3)	>46.3 (3)	50.0 (2)	52.7 (3)
K_2O	3.1 (1)	3.1 (1)	1.9 (1)	3.4 (1)	1.7 (1)	1.6 (1)	1.3 (1)	1.1 (1)
CaO	8.5 (1)	>8.3 (1)	9 (1)	<0.1	2.5 (1)	2.7 (1)	2.9 (1)	3.0 (1)
TiO_2	11.0 (3)	8.9 (2)	6.3 (1)	>7.1 (2)	31.2 (3)	23.7 (3)	15.8 (3)	13.2 (2)
FeO	0.1 (1)	0.2 (1)	0.3 (1)	b.d.	4.4 (2)	4.1 (2)	4.5 (2)	4.5 (2)
total	100.1	99.8	99.6	100.0	98.9	98.2	99.0	99.0

Trace elements rutiles (ppm)

	MHD15_1 (n = 11)	HD4_4 (n = 9)	HD2_4 (n = 10)	MHD16_1 (n = 4)	RT10-Na (n = 4)	RT10–20 (n = 4)	RT10–40 (n = 4)	RT10–40H (n = 4)
La	0.09 (7)	0.069 (57)	0.036 (24)	<0.04				
Ce	0.36 (17)	0.6 (2)	0.080 (77)	2.8 (3)				
Pr	0.11 (9)	<0.4	0.06 (2)	<0.05				
Sm	0.53 (33)	<0.5	0.5 (2)	0.24 (5)				
Gd	1.1 (10)	0.8 (6)	0.75 (58)	<1.0				
Lu	15.7 (10)	13.9 (8)	10.3 (11)	0.09 (5)				
Co	7.1 (9)	11.9 (10)	<0.18	b.d.	1.0 (1)	2.1 (2)	3.3 (3)	4.1 (9)
Cu	13.1 (27)	12.8 (18)	11.3 (39)	15.6 (40)	12.4 (12)	13.1 (24)	12.1 (5)	13.2 (24)
Zn	18.2 (47)	21.1 (56)	17 (42)	22.4 (29)	14.2 (5)	14.6 (28)	12.8 (10)	15.6 (39)
Sr	1.1 (4)	1.1 (2)	1.0 (2)	1.5 (4)	1.1 (2)	1.1 (1)	0.7 (2)	0.95 (23)
V	284 (15)	42.7 (42)	291 (28)	108 (7)	9.2 (11)	12.2 (10)	25.2 (11)	41.3 (4)
Cr	10.4 (82)	195 (23)	724 (42)	24.0 (61)	56.5 (66)	78.1 (14)	204 (10)	49.9 (75)
W	1.1 (6)	20 (3)	228 (79)	63 (11)	6.1 (9)	15.3 (28)	113 (12)	4.0 (9)
Sb	0.6 (2)	1.3 (5)	0.067 (60)	1.4 (3)	11.0 (10)	9.5 (16)	13.3 (25)	0.8 (5)
Zr	2652 (46)	2592 (300)	3103 (223)	554 (19)	183 (7)	255 (2)	376 (10)	3949 (11)
Hf	2120 (93)	2006 (169)	2069 (131)	3443 (398)	151 (10)	195 (9)	289 (11)	317 (12)
Nb	4058 (161)	3139 (368)	2257 (205)	4987 (202)	2313 (27)	2571 (47)	2332 (40)	2192 (45)
Ta	9539 (1532)	7127 (832)	3280 (438)	4424 (532)	3518 (286)	3648 (876)	2889 (501)	2514 (437)
Th	0.17 (10)	0.23 (14)	0.24 (14)	<0.25	<0.1	0.094 (80)	<0.1	<0.1
U	12.5 (11)	21.7 (47)	73.6 (99)	130 (14)	21.4 (49)	32.1 (61)	59.8 (58)	21.9 (21)

Trace element glass (ppm)

	MHD15_1 (n = 5)	HD4_4 (n = 5)	HD2_4 (n = 5)	MHD16_1 (n = 5)	RT10-Na (n = 3)	RT10–20 (n = 3)	RT10–40 (n = 3)	RT10–40H (n = 3)
La	310 (5)	344 (4)	346 (6)	1.2 (2)				
Ce	759 (11)	825 (18)	830 (4)	1269 (112)				
Pr	471 (8)	505 (12)	527 (9)	0.34 (12)				
Sm	268 (7)	290 (4)	289 (6)	343 (12)				
Gd	1026 (26)	1145 (27)	1156 (12)	1.0 (5)				
Lu	481 (13)	553 (10)	546 (11)	0.22 (5)				
Co	122 (15)	369 (13)	6.3 (11)	n.d.	97.1 (24)	101 (2)	112.9 (8)	122 (2)
Cu	2.9 (6)	72 (3)	1.82 (44)	4.8 (5)	20 (2)	16.0 (28)	15.6 (23)	14.2 (10)
Zn	1.8 (12)	<0.6	<0.2	<0.4	4.8 (34)	3.3 (12)	<1.5	1.1 (10)
Sr	298 (2)	319 (4)	329.5 (59)	206 (14)	79.3 (34)	81.6 (29)	85.8 (5)	93.1 (19)
V	66 (2)	81 (2)	16.3 (15)	42 (11)	61.4 (27)	65.1 (26)	70.1 (27)	61.1 (7)
Cr	<1.4	<1.8	59.3 (36)	<0.3	11.9 (64)	5.7 (63)	11.5 (14)	<2.6
W	2.3 (5)	5.1 (7)	5.3 (12)	5.9 (46)	3.2 (12)	2.9 (7)	7.8 (21)	<0.7
Sb	0.3 (2)	2.1 (3)	0.42 (15)	4.4 (24)	6.5 (8)	5.3 (3)	7.7 (13)	1.2 (6)
Zr	650 (11)	540 (10)	401 (9)	63 (3)	165 (1)	135 (3)	102 (3)	96.7 (9)
Hf	354 (5)	264 (4)	195 (4)	288 (22)	94.1 (4)	72 (2)	56 (4)	50.3 (15)

Table 3. (Continued)

	Trace element glass (ppm)							
	MHD15_1 (n = 5)	HD4_4 (n = 5)	HD2_4 (n = 5)	MHD16_1 (n = 5)	RT10-Na (n = 3)	RT10–20 (n = 3)	RT10–40 (n = 3)	RT10–40H (n = 3)
Nb	181 (4)	77 (3)	23 (2)	98 (10)	264.6 (4)	179 (2)	94 (1)	70.3 (22)
Ta	119 (6)	37 (3)	16 (2)	39 (7)	147 (3)	75.2 (8)	38 (5)	21.9 (10)
Th	1230 (28)	1362 (25)	1370 (22)	64 (7)	86	82.2 (36)	89.7 (19)	89.5 (5)
U	31 (1)	8.7 (4)	342 (5)	34 (26)	107 (2)	75.5 (11)	46.4 (44)	15.9 (10)
	Partition coefficients							
	MHD15_1 D	HD4_4 D	HD2_4 D	MHD16_1 D	RT10-Na D	RT10–20 D	RT10–40 D	RT10–40H D
La	0.0031 (24)	0.00019 (17)	0.0001 (1)	<0.04				
Ce	0.00047 (22)	0.00073 (24)	0.00010 (9)	0.0023 (3)				
Pr	0.00024 (20)	<0.00076	0.00012 (5)	<0.15				
Sm	0.0020 (12)	<0.0016	0.0018 (7)	0.0007 (1)				
Gd	0.0011 (10)	0.00073 (57)	0.00066 (50)	<1.0				
Lu	0.038 (2)	0.025 (2)	0.018 (2)	0.4 (3)				
Co	0.058 (10)	0.032 (3)	<0.03		0.011 (1)	0.021 (2)	0.029 (3)	0.033 (7)
Cu	4.5 (13)	0.18 (3)	6.2 (26)	3.2 (9)	0.62 (8)	0.8 (2)	0.8 (1)	0.93 (18)
Zn	10.0 (72)	>35	>85	>56	3.0 (20)	4.5 (18)	>8.5	14.3 (141)
Sr[b]	0.0038 (13)	0.0036 (5)	0.0030 (7)	0.007 (2)	0.013 (2)	0.013 (1)	0.008 (3)	0.010 (3)
V	4.3 (3)	0.53 (5)	17.8 (24)	2.6 (7)	0.15 (2)	0.19 (2)	0.36 (2)	0.68 (6)
Cr	>7.5	>108	12.2 (10)	>80	4.8 (26)	13.7 (152)	17.7 (24)	>19
W	0.5 (3)	3.9 (8)	43 (18)	10.7 (86)	1.9 (7)	5.3 (15)	14.5 (41)	<5.7
Sb	2.1 (15)	0.60 (23)	0.16 (15)	0.32 (19)	1.7 (3)	1.8 (3)	1.7 (4)	0.63 (49)
Zr	4.1 (1)	4.8 (6)	7.7 (6)	8.8 (5)	1.1 (10)	1.89 (5)	3.7 (1)	4.1 (1)
Hf	6.0 (3)	7.6 (7)	10.6 (7)	12.0 (17)	1.6 (1)	2.7 (2)	5.2 (4)	6.3 (3)
Nb	22 (1)	41 (5)	96 (11)	51.1 (55)	8.7 (1)	14.4 (3)	24.7 (5)	31.2 (12)
Ta	80 (13)	195 (29)	210 (37)	113 (23)	24.0 (20)	49 (12)	76 (17)	115 (21)
Th	0.00014 (8)	0.00017 (11)	0.00017 (10)	<0.004	<0.001	0.0011 (10)	<0.001	<0.001
U	0.40 (4)	2.5 (6)	0.21 (3)	3.8 (29)	0.20 (5)	0.42 (8)	1.3 (2)	1.4 (2)

[a] Major elements were analyzed with the electron microprobe; trace elements were analyzed with laser ablation ICPMS. Major element analyses of rutiles also included Si, Mg, Na, Ca and K but were always below the limit of detection. b.d. = below detection limit; n = number of analyses; D = c (mineral)/c(melt), where c is the concentration in ppm.

[b] Sr partition coefficients must be regarded as maximum values as the $^{48}Ti + {}^{40}Ar$ interference on ^{88}Sr was not corrected. Uncertainties (standard deviation of the mean, 1σ) given in brackets as last significant digits. For example, 6.9 (11) must be read as 6.9 ± 1.1 and 0.01 (2) as 0.01 ± 0.02. Some analyses were below the limit of the detection. In this case partition coefficients must be regarded as minimum or maximum values (indicated by > or < symbols). These data are not plotted in Figures 2 and 3. Detection limits of mineral analyses critically depend on the signal length during laser ablation (here mostly a function of mineral size) and may therefore substantially vary.

Fe-saturated platinum wires minimized the loss of iron from the sample (Grove, 1981). Experimental run products were mounted in epoxy and carefully polished with a series of diamond pastes. Polished sections were carbon coated for electron microprobe analysis. Glasses and rutiles were analyzed for major elements with a Cameca electron microprobe (SX51) at Heidelberg University. For glasses we used an accelerating voltage of 15 kV and a beam current of 6 nA. To minimize alkali volatility the 1 μm diameter electron beam was rastered over an area of 10 × 12 μm. Counting times were 10 s on peak and 5 s on background for all elements. For rutile analyses an accelerating voltage of 15 kV, a beam current of 20 nA, and a beam with 1 μm in diameter were used. The counting times were identical, except for Al with 20 s on peak and 10 s on background. The standards used were albite (Na), K-feldspar (K), corundum (Al), periclase (Mg), wollastonite (Ca, Si) and rutile (Ti). The raw data were corrected with the 'PAP' software (Pouchou and Pichoir, 1985).

Trace element concentrations in rutiles and glasses were determined using Laser ablation inductively coupled mass spectrometry (LA-ICPMS) at the Eidgenössische Technische Hochschule in Zürich. The LA-ICP-MS system consisted of a 193 nm ArF Excimer laser (Lambda Physics, Göttingen, Germany) in combination with an ELAN 6100 ICP-MS (Perkin Elmer Corp., Norwalk, Connecticut). The system is described in detail by Günther et al. (1997). The diameter of the laser beam was set to 20 μm to allow several analyses on larger grains. For each analysis elements were analyzed in the mass spectrometer for a total time of 60s. The gas background was measured for 30s and the signals were acquired for ~10–30 s. The gas mixture used during each analysis consisted of pure helium, which was used in the sample cell and later mixed downstream with pure argon. Titanium was used as internal standard, which successfully reproduces trace element concentrations of the calibration standard NIST SRM 610 glass within a relative difference of ±10% or less from published values (Pearce et al., 1997).

3. RESULTS AND DISCUSSION

3.1. Partition Coefficients

The experimental run products contained only rutile crystals and silicate glass, no other accessory phases or quench crystals were found. The rutile crystals were generally much larger than 50 μm and showed no signs of zoning or mineral inclusions. Some crystals contain melt inclusions. Glasses were transparent and inclusion free. Figure 2 depicts some selected rutiles in our experimental charges.

Although there is a large body of trace element partitioning data in the literature (see Irving, 1978, and Green, 1994, for excellent summaries), there are few experimental data available for rutile/melt partitioning (Table 1). Moreover, most previous

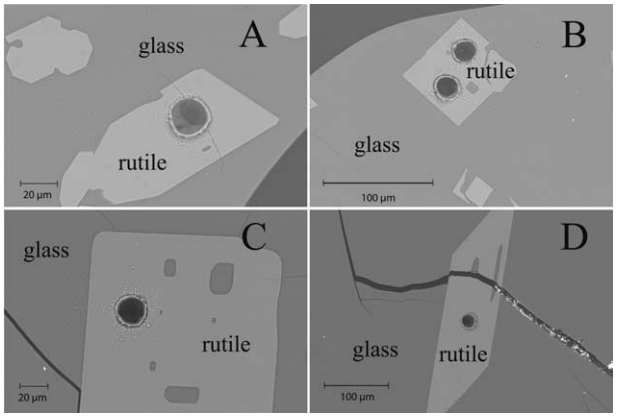

Fig. 2. Back-scattered electron images of experimental run products (A, HD2_4; B, HD4_4; C, RT10_20; D, RT10_40). The holes in the rutile crystals are laser ablation pits and are ~20 μm in diameter. Dark areas in rutiles are melt inclusions. Note that the cracks in some of the experimental run products were caused during the quench.

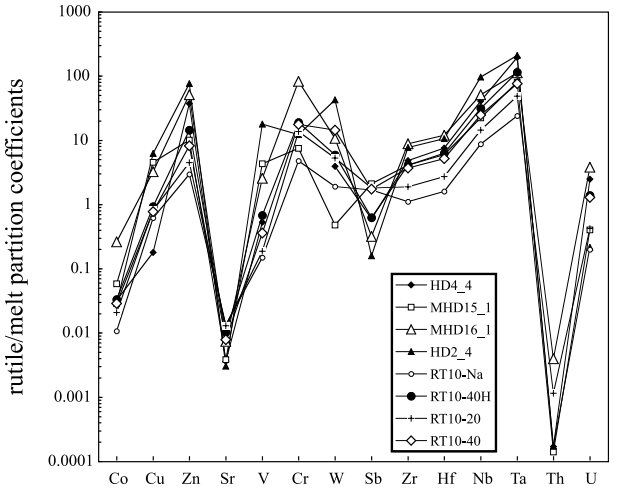

Fig. 3. All our new experimental rutile/melt partition coefficients. $D_{Nb} < D_{Ta}$, $D_{Hf} > D_{Zr}$ and $D_U > D_{Th}$ in all experiments. For clarity, error bars are not depicted. Note that large variations in D_W, D_{Sb} and possibly D_{Co} occur systematically with changing fO_2. This may explain the large range of our measured values. See text for details.

studies focused on a small number of trace elements (Green and Pearson, 1987; Jenner et al., 1993; Green, 1995, 2000; Foley et al., 2000; Horng and Hess, 2000; Schmidt et al., 2004). None of these studies presents a comprehensive set of partition coefficients for all HFSEs, which was one of the aims of this study. Moreover, we also intended to study the partitioning of U, Th, and some selected transition metals (W, Sb, V, Co), which are known to be concentrated in rutile (Zack et al., 2002, 2004). Some of these elements may also be of interest in subduction zone processes (e.g., Sb in island arc volcanic rocks has been reported to decrease with increasing depth of the subducting slab; Ryan et al., 1995; Hattori et al., 2002; Hattori and Guillot, 2003). None of the previous studies contain partitioning data for these elements. Also, as recent studies have revived the interest in the melt composition as a significant factor controlling element partitioning (e.g., Kohn and Schofield, 1994; Horng and Hess, 2000; Linnen and Keppler, 2002; O'Neill and Eggins, 2002), we have also investigated rutile/melt trace element partitioning in systems with very different melt compositions (Table 3).

Major and trace element concentrations of the run products and calculated partition coefficients for rutile/melt pairs are listed in Table 3. The partition coefficients are depicted in Figures 3 and 4. The high field strength elements (Zr, Hf, Nb, Ta) and the transition metals Cr and Zn are compatible in rutile (i.e., $D > 1$) in all experiments whereas Sr, Th and Co are incompatible. Moreover, it was possible to determine partition coefficients in several experiments where the particular element had not been doped or were added in much lower concentrations (Table 2). Partition coefficients from these experiments are in excellent agreement with data from experiments where the trace element was added in higher concentrations. As mentioned above, this agreement indicates that Henry's law was followed in our experiments. Other transition metals (W, Sb, V) vary substantially which is interpreted to be mainly caused by changes in oxygen fugacity (fO_2). It is interesting to note that W partition coefficients decrease with increasing fO_2 whereas Sb partition coefficients exhibit the opposite behavior (Table 3). Tungsten in geological environments displays two oxidation states, W^{4+} and W^{6+} (Henderson, 1982), but the redox behavior of W in silicate melts (and crystals) is not well understood. In our experiments we expect a mixture of W^{4+} and W^{6+} at higher oxygen fugacities and predominantly W^{4+} in the experiments at rather low oxygen fugacity. Similarly, antimony in geological environments is either Sb^{3+} or Sb^{5+}, but in most cases one would expect a mixture of both valence states. At higher fO_2 (e.g., run MHD15_1, $\log fO_2 = -0.96$) we expect mostly Sb^{5+}, whereas at lower fO_2 antimony should be mostly Sb^{3+}(e.g., run HD2_4, $\log fO_2 = -11.3$). Again, valence states (and indeed the geochemistry) of Sb are not well understood

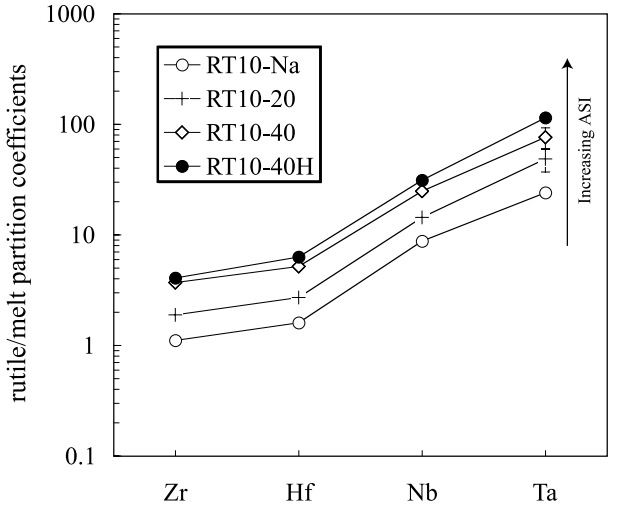

Fig. 4. Rutile/melt partition coefficients from our experiments with strongly differing melt compositions. All HSFE partition coefficients increase with increasing alumina saturation index (ASI) of the melt. This may be due to complexation of the HFSE with aluminium in melts, see text for discussion. Error bars (1σ) only depicted when larger than symbols.

(Jochum and Verma, 1996; Righter et al., 2001; Schmid et al., 2003). Although the response of vanadium to different redox states is slightly better understood (Canil, 1997, 1999, 2002; Gaetani and Grove, 1997) the partitioning of V in our experiments is much more difficult to interpret, as we observe the lowest D_V under oxidizing conditions where V^{4+} and V^{5+} should be the predominant species (Tables 2 and 3). The highest D_V was observed in andesitic compositions in very reducing compositions (run HD2_4), which we interpret as due to V^{5+} as dominant species (Platt and Mitchell, 1996; Gaetani and Grove, 1997; Canil, 1999). The other experiments show intermediate D_V at relatively oxidizing conditions (Table 2), which indicates that V exhibits a more or less constant mixture of valence (mostly V^{4+} and V^{5+}) states in these runs (MHD15 and HD4_4) with no significant effects of fO_2 on partition coefficients (Table 3). Further work is clearly needed to better understand the partitioning of vanadium between key minerals such as rutile or ilmenite and melts, especially as rutile and ilmenite are known to incorporate higher concentrations of V. Similarly, no systematic dependence of D_{Cu}, D_{Cr} on fO_2 was found (Table 3), which is also interpreted to be due to predominantly Cu^{2+} and Cr^{3+} in our experiments. In the case for Cr, it is well established that extremely reducing conditions are needed to reduce Cr^{3+} to Cr^{2+} (Li et al., 1995; Holzheid and O'Neill, 1995), and our experiments were not reducing enough to stabilize Cr^{2+}.

In this context we would like to caution the reader that we encountered significant experimental problems with volatile elements such as W, Sb, Mo, Sn, and Pb. Note that our main aim was to determine HFSE partition coefficients so that our experiments were not optimized to study volatile elements. Lead, Mo, and Sn were indeed quantitatively lost during the experiments so that no meaningful partition coefficients could be calculated. This appears to be caused by volatility, but alloying of Pb, Mo, and Sn with the platinum wire loop is an alternative explanation for the observed loss. Similar problems, to a somewhat lesser extent, occurred with Sb and W (Tables 2 and 3). As our W and Sb partition coefficients varied systematically and neither glasses nor rutile crystals were zoned within the analytical uncertainties, we decided to use our Sb and W data, although these partition coefficients should only be used with caution. The volatile elements Sb and W were likely to be lost during the initial stages of the experiments (i.e., at high temperatures). Further loss of Sb and W during the course of the experiments (i.e., during cooling to lower temperatures) was probably minimal. This is why equilibrium between rutile and melts was attained (even for Sb and W) at the final run temperature. However, we recognize that better experimental work is clearly needed to constrain the partitioning of volatile elements such as Sb, W, Mo, and Pb in silicate systems.

It has been proposed that melt composition is a significant factor controlling partition coefficients (Watson, 1976; Ryerson and Hess, 1978; Lesher, 1986; Nielsen et al., 1992; Kohn and Schofield, 1994; Horng and Hess, 2000; Kushiro and Mysen, 2002; Linnen and Keppler, 2002; O'Neill and Eggins, 2002; Klemme and Dalpé, 2003; Prowatke and Klemme, 2005; Schmidt et al., 2004). A recent study that investigated rutile/melt partition coefficients in haplogranitic compositions found strongly increasing D_{Nb} and D_{Ta} with decreasing $K_2O/(K_2O + Al_2O_3)$ of coexisting melts. Horng and Hess (2000) argued that the compositional dependence of their partition coefficients was caused by different complexation mechanisms of Nb and Ta in melts in peralkaline and peraluminous melts, respectively. Moreover, Horng and Hess (2000) found that the substitution mechanism by which Nb^{5+} and Ta^{5+} are incorporated into the rutile structure [Nb^{5+} (or Ta^{5+}) + Al^{3+} = 2 Ti^{4+}] has additional control over partition coefficients. They concluded that in systems with high alumina contents (or aluminium activity) higher contents of Nb (or Ta) may be incorporated in rutiles by coupled substitution. Alternative substitution mechanisms in more complex systems are Fe^{2+} + Nb^{5+} (or Ta^{5+}) = Ti^{4+} + Al^{3+} or Fe^{2+} + 2 Nb^{5+} (or 2 Ta^{5+}) = 3 Ti^{4+}, or coupled substitution with vacancies 4 Nb^{5+} (or Ta^{5+}) + □ = 5 Ti^{4+} (Horng and Hess, 2000).

We present new Zr and Hf partition coefficients. The incorporation of Zr^{4+} and Hf^{4+} into rutile is an isovalent exchange that should not be affected by the substitution mechanism (i.e., the aluminium content of crystals or melts). If the substitution mechanism were a significant factor in this context one would expect no significant changes of D_{Zr} or D_{Hf}. Nevertheless, we observe an increase of D_{Zr} and D_{Hf} with increasing alumina saturation index in our experiments (Fig. 4) in an identical manner to D_{Nb} and D_{Ta}. This implies that it is not the substitution mechanism that determines the compositional dependence of partition coefficients observed in our study but the melt composition itself. Complexation of the HFSEs as proposed by Horng and Hess (2000) is a viable mechanism in this context. It should be noted that Horng and Hess (2000) found D_{Ta} always larger than D_{Nb} in their experiments, which is in good agreement with most previous studies on rutile/melt partitioning and with our data (Figs. 1 and 3). Although they always report $D_{Nb} < D_{Ta}$, Schmidt et al. (2004) find increasing D_{Nb}/D_{Ta} with increasing degree of polymerization of silcate melts. If the ionic radius of Nb^{5+} is indeed larger than the ionic radius of Ta^{5+} (Tiepolo et al., 2000), exactly the opposite effect would be expected, as elements with small ionic radius and high charge (such as Nb^{5+} and Ta^{5+}) are expected to partition preferentially into a depolymerized melts (Ryerson and Hess, 1978). Our data do not support the observations of Schmidt et al. (2004) (Table 3), as we find no systematic variation of D_{Nb}/D_{Ta} with melt composition. As mentioned by Prowatke and Klemme (2005), not much is known about the local environment of trace elements in silicate melts and more direct determinations of the local environment of Nb and Ta (and other HFSEs) using synchrotron X-ray spectroscopy are needed to shed further light on these matters (e.g., Farges et al., 1996; Farges, 1997, 1999).

We have also investigated the partitioning of some selected REEs between rutile and melts (Table 3). As expected, the REE do not readily enter the rutile structure and partition coefficients are vanishingly low, with D_{Lu} slightly higher than D's for the light REE or middle REE. We also present the first measured rutile-melt partition coefficients for Th and U. We find D_{Th} consistently lower than D_U. As the experiments were performed at different oxygen fugacities ($-11.3 < \log fO_2 < -0.96$), one would expect mainly U^{6+} to be present in the oxidizing runs (e.g., run MHD15_1, log fO_2 = −0.96), whereas U^{4+} should be the dominant species in the reducing experiments (e.g., run HD2_4, log fO_2 = −11.3). Previous work has clearly shown that the geochemical behavior of U^{6+}

is rather different from U^{4+}, due mainly to different ionic radii and the difference in charge (e.g., Bailey and Ragnarsdottir, 1994). Nevertheless, D_U does not change much in our experiments and the effect of fO_2 on D_U is not as strong as we expected. This behavior is confirmed by analyses of rutiles from very different tectonic environments. Although these rutiles were probably equilibrated under different redox potentials, all the crystals analyzed contain much more U than Th (Zack et al., 2002, 2004). This was previously interpreted to be caused by fluids or melts that contain significantly more U than Th, which is a fair assumption given the fact that U^{6+} is much more soluble in fluids compared to Th (cf. Bailey and Ragnarsdottir, 1994). Our data shows, however, that high U/Th in rutile may also be caused by the preferential partitioning of U into the rutile structure.

3.2. Implications for Subduction Zone Processes

3.2.1. Rutile as major control of Nb/Ta in subduction zones?

As most volcanic rocks in subduction zones, adakites are characterized by the relative depletion of HFSEs when compared to volcanic rocks from other tectonic settings such as mid–ocean-ridge basalts or ocean-island basalts. Adakites are often considered as modern analogues to Archaean gneisses of trondhjemitic, tonalitic and granodioritic (TTG) composition (Martin, 1987, 1999; Defant and Drummond, 1990; Drummond and Defant, 1990). Most TTGs and adakites show low Nb/Ta and high Zr/Sm (see Foley et al., 2002). Many studies conclude that rutile may be the key mineral phase that selectively retains the HFSEs during melting or dehydration of the subducting slab at elevated pressures (e.g., McCulloch and Gamble, 1991; Brenan et al., 1994, 1995; Münker, 1998; Stalder et al., 1998; Klemme et al., 2002). Recently, Foley et al. (2002) challenged this view suggesting that the chemical characteristics of TTGs are better explained by melting of garnet amphibolite. This alternative has been criticized by Rapp et al. (2003) who presented experimental evidence for the origin of TTGs by melting of eclogite with subchondritic Nb/Ta.

The stability of rutile in subducted lithosphere is a complex function of bulk composition, temperature, and pressure (Green, 1981; Ryerson and Watson, 1987; Klemme et al., 2002; Zhang et al., 2003). Moreover, the composition of the subducted lithosphere varies substantially in terms of Ti and exhibits a wide range of Nb/Ta ratios (Melson et al., 1976; Münker, 1998; Klemme et al., 2002; Rapp et al., 2003). If the bulk rock composition of the eclogite (or amphibolite) is rich in TiO_2 and the degree of partial melting is not too high (Klemme et al., 2002), rutile is expected to remain residual during partial melting of eclogite, perhaps even in amphibolite as rutile-bearing amphibolites in metamorphic rocks indicate (e.g., Zhao et al., 1999; Bebout and Barton, 2002; Puga et al., 2002; Mitra and Bidyananda, 2003). Experimental evidence combined with thermal models indicates that in Archaean subduction zones, melting should occur within the amphibolite or eclogite stability field (Rapp et al., 1991, 1999, 2003; Rapp and Watson, 1995; Barth et al., 2002; Foley et al., 2002; Klemme et al., 2002). Our data and most previous studies show that the residue will be become progressively depleted in Nb (i.e., low Nb/Ta). Eclogites that have suffered partial melting cannot, therefore, be the reservoir with superchondritic Nb/Ta that has been proposed on the basis of mass balance constraints (Kamber and Collerson, 2000; Rudnick et al., 2000). Rutile/fluid partition coefficients for Nb and Ta are much less well constrained. Early experiments showed rutile/fluid $D_{Nb}/D_{Ta} > 1$ (Brenan et al., 1994), whereas Stalder et al. (1998) could not determine any significant difference between D_{Nb} and D_{Ta}. Recent experiments by Green and Adam (2003) indicated that rutile/fluid $D_{Nb}/D_{Ta} < 1$. If correct, this further supports the notion that subducted eclogite cannot be the reservoir with superchondritic Nb/Ta. Note that rutile/fluid partition coefficients are much more difficult to determine experimentally than rutile/melt partition coefficients.

Summarizing, the partition coefficients between rutile and melt (or fluid) reinforce the view that the continental crust with its low Nb/Ta cannot be the melting products of average subducted eclogite (Foley et al., 2002), only partial melting of subducted crust with extremely low Nb/Ta could result in melts with sufficiently low Nb/Ta (Rapp et al., 2003).

3.2.2. U-Series Disequilibria in Arc Volcanics

U-Th isotope disequilibria are commonly employed to constrain the timing of element transfer processes in subduction zones (Turner et al., 1996, 1998; Elliott et al., 1997; Hawkesworth et al., 1997). Many island arc volcanics show significant ^{238}U excess that has been explained by enrichment of U over Th in the source of these lavas (e.g., Turner et al., 1996, 1998; Elliott et al., 1997; Hawkesworth et al., 1997). As U^{6+} is much more soluble in fluids than Th (Bailey and Ragnarsdottir, 1994; Brenan et al., 1994, 1995) several studies have interpreted U-Th isotope disequilibria to reflect the time elapsed from the fluid-release from the dehydrating subducting lithosphere (e.g., Turner et al., 1996, 1998; Elliott et al., 1997; Hawkesworth et al., 1997). Other subduction zone lavas, however, show an excess of ^{230}Th over ^{238}U (Sigmarsson et al., 1998). These lavas, so-called adakites, are characterized by high La/Yb and Sr/Y and are thought to be generated by partial melting of the subducted lithosphere (Defant and Drummond, 1990; Drummond and Defant, 1990; Stern and Kilian, 1996; Yogodzinski and Kelemen, 1998). Sigmarsson et al. (1998) explained the observed excesses of ^{230}Th over ^{238}U by partial melting in the presence of residual rutile. Their interpretations were somewhat hampered by the fact that no U or Th partition coefficients for rutile were available. However, our rutile partition coefficients agree with their conclusions as we find $D_U \gg D_{Th}$, which is in good agreement with theoretical considerations (Sigmarsson et al., 1998; Blundy and Wood, 2003). Our new rutile partition coefficients should enable more precise interpretation of U-series disequilibria in subduction zone volcanics.

Most studies of U-series disequilibria have focussed on $^{230}Th/^{238}U$. As analytical techniques have been substantially improved over the last few years, a few recent studies have also investigated ^{226}Ra-^{230}Th and ^{231}Pa-^{235}U (Chabaux and Allègre, 1994; Pickett and Murrell, 1997; Bourdon et al., 1999; Chabaux et al., 1999; Turner et al., 2000; Turner et al., 2001). The latter are especially extremely difficult to measure as Pa abundances are rather low. Interpretations of ^{231}Pa-^{235}U systematics are hampered by our lack of understanding of Pa geochemistry. As Pa is highly radioactive and cannot be han-

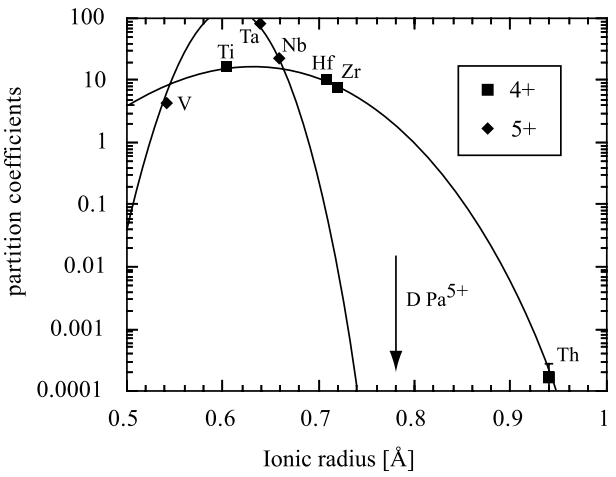

Fig. 5. Rutile/melt partition coefficients for the quadrivalent (Ti, Zr, Hf and U^{4+}) in the most reduced experiment) and pentavalent elements (Nb, Ta, and V^{5+}) of our most oxidized experiment. Note that we used an ionic radius for Nb^{5+} of 0.66Å (Tiepolo et al., 2000; Blundy and Wood, 2003), all other ionic radii are from (Shannon, 1976). The approximate value of D Pa^{5+} is indicated by the arrow and should be well below 0.0001. Error bars (1σ) only depicted when larger than symbols.

dled in conventional experimental and geochemical laboratories, partition coefficients for Pa will probably never be determined experimentally. Based on theoretical considerations, however, rutile has been suggested as a phase with a potential to contain significant amounts of Pa (Blundy and Wood, 2003). Our most oxidizing partitioning experiment includes partition coefficients for three pentavalent elements (Nb, Ta and V^{5+}). As Pa is also pentavalent in geological environments, our data permit estimation of D_{Pa} for rutile. To do this, we have plotted partition coefficients for pentavalent elements in Figure 5. Extrapolating our data to Pa^{5+} (with an ionic radius of 0.78Å; Shannon, 1976), we suggest that D_{Pa} is vanishingly small for rutile ($D_{Pa} \ll 0.001$). Note that this rather crudely estimated partition coefficient is much lower than previous estimates (Blundy and Wood, 2003; Dosseto et al., 2003). Our data imply that rutile should not be able to incorporate significant amounts of Pa and is, therefore, not likely to lower $^{231}Pa/^{235}U$ significantly (Dosseto et al., 2003).

Acknowledgments—We are indebted to Hans Peter Meyer for his help with the electron microprobe at Heidelberg University. Furthermore, we would like to thank T. Zack, R. Altherr, H. Marschall, T. Ludwig, D. Lattard, H. Kleinschmidt, H. Meyer, I. Glass and many others at Heidelberg University for discussions and support at various stages of the project. We would also like to thank S.F. Foley, T.H. Green, and J.C. Ayers for thorough and helpful reviews. We are indebted to D. Lattard for access to the experimental laboratories at Heidelberg University.

Associate editor: C. Neal

REFERENCES

Ayers J. C. (1998) Trace element modeling of aqueous fluid–peridotite interaction in the mantle wedge of subduction zones. *Contrib. Mineral. Petrol.* **132,** 390–404.

Bailey E. H. and Ragnarsdottir K. V. (1994) Uranium and thorium solubilities in subduction zone fluids. *Earth Planet. Sci. Lett.* **124,** 119–129.

Barth M. G., Foley S. F., and Horn I. (2002) Partial melting in Archean subduction zones: Constraints from experimentally determined trace element partition coefficients between eclogitic minerals and tonalitic melts under upper mantle conditions. *Precam. Res.* **113,** 323–340.

Bebout G. E. and Barton M. D. (2002) Tectonic and metasomatic mixing in a high-T, subduction-zone melange—Insights into the geochemical evolution of the slab-mantle interface. *Chem. Geol.* **187,** 79–106.

Blundy J. D. and Wood B. J. (1994) Prediction of crystal-melt partition coefficients from elastic moduli. *Nature* **372,** 452–454.

Blundy J. D. and Wood B. J. (2003) Mineral-melt partitioning of uranium, thorium and their daughters. *Rev. Mineral.* **52,** 59–123.

Bourdon B., Turner S., and Allegre C. J. (1999) Melting dynamics beneath the Tonga-kermadec island arc inferred from ^{231}Pa-^{235}U systematics. *Science* **286,** 2491–2493.

Brenan J. M., Shaw H. F., Phinney D. L., and Ryerson F. J. (1994) Rutile-aqueous fluid partitioning of Nb, Ta, Hf, Zr, U and Th—Implications for high-field strength element depletions in island arc basalts. *Earth Planet. Sci. Lett.* **128,** 327–339.

Brenan J. M., Shaw H. F., Ryerson F. J., and Phinney D. L. (1995) Mineral-aqueous fluid partitioning of trace elements at 900 degrees C and 2.0 GPa—Constraints on the trace element chemistry of mantle and deep crustal fluids. *Geochim. Cosmochim. Acta* **59,** 3331–3350.

Canil D. (1997) Vanadium partitioning and the oxidation state of Archean komatiite magmas. *Nature* **389,** 842–845.

Canil D. (1999) Vanadium partitioning between orthopyroxene, spinel and silicate melt and the redox states of mantle source regions for primary magmas. *Geochim. Cosmochim. Acta* **63,** 557–572.

Canil D. (2002) Vanadium in peridotites, mantle redox and tectonic environments: Archean to present. *Earth Planet. Sci. Lett.* **195,** 75–90.

Chabaux F. and Allègre C. J. (1994) ^{238}U-^{230}Th-^{226}Ra disequilibria in volcanics—A new insight into melting conditions. *Earth Planet. Sci. Lett.* **126,** 61–75.

Chabaux F., Hemond C., and Allegre C. (1999) ^{238}U-^{230}Th-^{226}Ra disequilibria in the Lesser Antilles arc: Implications for mantle metasomatism. *Chem. Geol.* **153,** 171–185.

Corrigan G. and Gibb F. G. F. (1979) Loss of Fe and Na from a basaltic melt during experiments using the wire-loop method. *Min. Mag.* **43,** 121–126.

Davies J. H. and Stevenson D. J. (1992) Physical model of source region of subduction zone volcanics. *J. Geophys. Res.* **97,** 2037–2070.

Defant M. J. and Drummond M. S. (1990) Derivation of some modern arc magmas by partial melting of young subducted lithosphere. *Nature* **347,** 662–665.

Deines P., Nafziger R. H., Ulmer G. C., and Woermann E. (1974) *Temperature-Oxygen Fugacity Tables for Selected Gas Mixtures in the System C-H-O at One Atmosphere Total Pressure.* Earth and Mineral Science Exploration Station Bulletin, 88. Pennsylvania State University, University Park.

Dinsdale A. T. (1991) Thermal and physical properties of pure metals. *Calphad* **15,** 31719.

Donaldson C. H. and Gibb F. G. F. (1979) Changes in sample composition during experiments using the wire-loop technique. *Min. Mag.* **43,** 115–115.

Dosseto A., Bourdon B., Joron J.-J., and Dupre B. (2003) U-Th-Pa-Ra study of Kamchatka arc: New constraints on the genesis of arc lavas. *Geochim. Cosmochim. Acta* **67,** 2857–2877.

Drummond M. S. and Defant M. J. (1990) A model for trondhjemite-tonalite-dacite genesis and crustal growth via slab melting: Archean to modern comparisons. *J. Geophys. Res.* **95,** 21503–21521.

Elliott T., Plank T., Zindler A., White W., and Bourdon B. (1997) Element transport from slab to volcanic front at the Mariana arc. *J. Geophys. Res.* **102,** 14991–15019.

Farges F. (1997) Coordination of Ti^{4+} in silicate glasses: A high-resolution XANES spectroscopy study at the Ti K edge. *Am. Mineral.* **82,** 36–43.

Farges F. (1999) A Ti K-edge EXAFS study of the medium range environment around Ti in oxide glasses. *J. Non-Cryst. Solids* **244,** 25–33.

Farges F., Brown G. E., and Rehr J. J. (1996) Coordination chemistry of Ti(IV) in silicate glasses and melts. 1. XAFS study of titanium coordination in oxide model compounds. *Geochim. Cosmochim. Acta* **60,** 3023–3038.

Foley S. F., Barth M. G., and Jenner G. A. (2000) Rutile/melt partition coefficients for trace elements and an assessment of the influence of rutile on the trace element characteristics of subduction zone magmas. *Geochim. Cosmochim. Acta* **64,** 933–938.

Foley S. F., Tiepolo M., and Vannucci R. (2002) Growth of early continental crust controlled by melting of amphibolite in subduction zones. *Nature* **417,** 837–840.

Gaetani G. A. and Grove T. L. (1997) Partitioning of moderately siderophile elements among olivine, silicate melt and sulfide melt: Constraints on core formation in the Earth and Mars. *Geochim. Cosmochim. Acta* **61,** 1829–1846.

Green T. H. (1981) Experimental evidence for the role of accessory phases in magma genesis. *J. Volc. Geotherm. Res.* **10,** 405–422.

Green T. H. (1994) Experimental studies of trace-element partitioning applicable to igneous Petrogenesis—Sedona 16 years later. *Chem. Geol.* **117,** 1–36.

Green T. H. (1995) Significance of Nb/Ta as an indicator of geochemical processes in the crust-mantle system. *Chem. Geol.* **120,** 347–359.

Green T. H. (2000) New partition coefficient determinations pertinent to hydrous melting processes in subduction zones. In *State of the Arc 2000: Processes and Timescales,* (eds. J. P. Davidson, J. A. Gamble and R. C. Price) pp. 92–95. Wellington.

Green T. H. and Pearson N. J. (1987) An experimental study of Nb and Ta partitioning between Ti-rich minerals and silicate liquids at high pressure and temperature. *Geochim. Cosmochim. Acta* **51,** 55–62.

Green T. H. and Adam J. (2003) Experimentally-determined trace element characteristics of aqueous fluid from partially dehydrated mafic oceanic crust at 3.0 GPa, 650–700 degrees C. *Eur. J. Mineral.* **15,** 815–830.

Grove T. L. (1981) Use of FePt alloys to eliminate the iron loss problem in 1 atmosphere gas mixing experiments: Theoretical and practical considerations. *Contrib. Mineral. Petrol.* **78,** 298–304.

Günther D., Frischknecht R., Heinrich C. A., and Kahlert H. J. (1997) Capabilities of an Argon Fluoride 193 nm excimer laser for laser ablation inductively coupled plasma mass spectrometry microanalysis of geological materials. *J. Anal. Atom. Spec.* **12,** 939–944.

Hattori K. H., Arai S., and Clarke D. B. (2002) Selenium, tellurium, arsenic and antimony contents of primary mantle sulfides. *Can. Mineral.* **40,** 637–650.

Hattori K. H. and Guillot S. (2003) Volcanic fronts form as a consequence of serpentinite dehydration in the forearc mantle wedge. *Geology* **31,** 525–528.

Hawkesworth C. J., Turner S. P., McDermott F., Peate D. W., and van Calsteren P. (1997) U-Th isotopes in arc magmas: Implications for element transfer from subducted crust. *Science* **276,** 551–555.

Henderson P. (1982) *Inorganic Geochemistry.* Pergamon Press.

Holzheid A. and O'Neill H. St. C. (1995) The Cr-Cr_2O_3 oxygen buffer and the free energy of formation of Cr_2O_3 from high-temperature electrochemical measurements. *Geochim. Cosmochim. Acta* **59,** 475–479.

Horng W. S. and Hess P. C. (2000) Partition coefficients of Nb and Ta between rutile and anhydrous haplogranite melts. *Contrib. Mineral. Petrol.* **138,** 176–185.

Irving A. J. (1978) A review of experimental studies of crystal/liquid trace element partitioning. *Geochim. Cosmochim. Acta* **42,** 743–770.

Jenner G. A., Foley S. F., Jackson S. E., Green T. H., Fryer B. J., and Longerich H. P. (1993) Determination of partition coefficients for trace elements in high-pressure-temperature experimental run products by laser ablation microprobe—Inductively coupled plasma mass spectroscopy. *Geochim. Cosmochim. Acta* **58,** 5099–5103.

Jochum K. P. and Verma S. P. (1996) Extreme enrichment of Sb, Tl and other trace elements in altered MORB. *Chem. Geol.* **130,** 289–299.

Kamber B. S. and Collerson K. D. (2000) Role of hidden deeply subducted slabs in mantle depletion. *Chem. Geol.* **166,** 241–254.

Kelemen P. B., Rilling J. L., Parmentier E. M., Mehl L. and Hacker B. R. (2004) Thermal structure due to solid-state flow in the mantle wedge beneath arcs. In *Inside the Subduction Factory* (ed. J. Eiler), pp. 293–311. Monograph 138. American Geophysical Union.

Klemme S., Blundy J. D., and Wood B. J. (2002) Experimental constraints on major and trace element partitioning during partial melting of eclogite. *Geochim. Cosmochim. Acta* **66,** 3109–3123.

Klemme S. and Dalpé C. (2003) Trace element partitioning between apatite and carbonatite melt. *Am. Mineral.* **88,** 639–646.

Klemme S. and Meyer H.-P. (2003) Trace element partitioning between baddeleyite and carbonatite melt at high pressures and high temperatures. *Chem. Geol.* **199,** 233–242.

Kohn S. C. and Schofield P. F. (1994) The importance of melt composition in controlling trace-element behavior—An experimental study of Mn and Zn partitioning between forsterite and silicate melts. *Chem. Geol.* **117,** 73–87.

Kushiro I. and Mysen B. O. (2002) A possible effect of melt structure on the Mg-Fe^{2+} partitioning between olivine and melt. *Geochim. Cosmochim. Acta* **66,** 2267–2272.

Lesher C. E. (1986) Effects of silicate liquid composition on mineral-liquid element partitioning from soret diffusion studies. *J. Geophys. Res.* **91,** 6123–6141.

Leybourne M. I., VanWagoner N., and Ayres L. D. (1999) Partial melting of a refractory subducted slab in a paleoproterozoic island arc: Implications for global chemical cycles. *Geology* **27,** 731–734.

Li J.-P., O'Neill H. St. C., and Seifert F. (1995) Subsolidus phase relations in the system MgO-SiO_2-Cr-O in equilibrium with metallic Cr and their significance for the petrochemistry of chromium. *J. Petrol.* **36,** 107–132.

Linnen R. L. and Keppler H. (1997) Columbite solubilty in granitic melts: Consequences for the enrichment and fractionation of Nb and Ta in the Earth's crust. *Contrib. Mineral. Petrol.* **128,** 213–227.

Linnen R. L. and Keppler H. (2002) Melt composition control of Zr/Hf fractionation in magmatic processes. *Geochim. Cosmochim. Acta* **66,** 3293–3301.

Martin H. (1987) Petrogenesis of Archean trondhjemites, tonalites and granodiorites from eastern Finland—Major and trace-element geochemistry. *J. Petrol.* **28,** 921–953.

Martin H. (1999) Adakitic magmas: Modern analogues of Archaean granitoids. *Lithos* **46,** 411–429.

McCallum I. S. and Charette M. P. (1978) Zr and Nb partition coeffcients: Implications for the genesis of mare basalts, KREEP and sea floor basalts. *Geochim. Cosmochim. Acta* **42,** 859–869.

McCulloch M. T. and Gamble J. A. (1991) Geochemical and geodynamical constraints on subduction zone magmatism. *Earth Planet. Sci. Lett.* **102,** 358–374.

Melson W. G., Vallier T., Wright T., Byerly G. and Nelson J. (1976) Chemical diversity of abyssal volcanic glass erupted along Pacific, Atlantic and Indian Ocean spreading centers. In *The Geophysics of the Pacific Ocean Basin and Its Margin* (eds. G. H. Sutton, M. H. Manghnani and R. Moberly), pp. 351–361. Monograph 19. American Geophysical Union.

Mitra S. and Bidyananda M. (2003) Cation distribution in calcic amphiboles from the Nuggihalli Greenstone belt, S. India and its geological significance. *N. Jb. Min. Abh.* **178,** 173–196.

Münker C. (1998) Nb/Ta fractionation in a Cambrian arc back arc system, New Zealand: Source constraints and application of refined ICPMS techniques. *Chem. Geol.* **144,** 23–45.

Nielsen R. L., Gallahan W. E., and Newberger F. (1992) Experimentally determined mineral-melt partition-coefficients for Sc, Y and REE for olivine, orthopyroxene, pigeonite, magnetite and ilmenite. *Contrib. Mineral. Petrol.* **110,** 488–499.

O'Neill H. St. C. and Eggins S. M. (2002) The effect of melt composition on trace element partitioning: An experimental investigation of the activity coefficients of FeO, NiO, CoO, MoO_2 and MoO_3 in silicate melts. *Chem. Geol.* **186,** 151–181.

Peacock S. M. (1991) Numerical simulation of subduction zone pressure-temperature-time paths: Constraints of fluid production and arc magmatism. *Philos. Trans. R. Soc. A* **335,** 341–353.

Peacock S. M. (1996) Thermal and petrologic structure of subduction zones. In *Subduction: Top to Bottom* (eds. G. E. Bebout, D. W.

Scholl, S. H. Kirby and J. P. Platt), pp. 119–133. American Geophysical Union.

Pearce N. J. G., Perkins W. T., Westgate J. A., Gorton M. P., Jackson S. E., Neal C. R., and Chenery S. P. (1997) A compilation of new and published major and trace element data for NIST SRM 610 and NIST SRM 612 glass reference materials. *Geostand. Newslett.* **21,** 115–144.

Pickett D. A. and Murrell M. T. (1997) Observations of $^{231}Pa/^{235}U$ disequilibrium in volcanic rocks. *Earth Planet. Sci. Lett.* **148,** 259–271.

Platt R. G. and Mitchell R. H. (1996) Transition metal rutiles and titanates from the Deadhorse Creek diatreme complex, northwestern Ontario, Canada. *Min. Mag.* **60,** 403–414.

Pouchou J. L. and Pichoir F. (1985) "PAP" procedure for improved quantitative microanalysis. *Microbeam Anal.* **54,** 104–106.

Prowatke S. and Klemme S. (2005) The effect of melt composition on the partitioning of trace elements between titanite and silicate melt. *Geochim. Cosmochim. Acta,* **69,** 695–709.

Puga E., Cruz M. D. R., and De Federico A. D. (2002) Polymetamorphic amphibole veins in metabasalts from the Betic Ophiolitic Association at Cobdar, southeastern Spain: Relics of ocean-floor metamorphism preserved through the Alpine orogeny. *Can. Mineral.* **40,** 67–83.

Rapp R. P., Watson E. B., and Miller C. F. (1991) Partial melting of amphibolite/eclogite and the origin of Archean trondhjemites and tonalites. *Precamb. Res.* **51,** 1–25.

Rapp R. P. and Watson E. B. (1995) Dehydration melting of metabasalt at 8–32 kbar: Implications for continental growth and crust-mantle recycling. *J. Petrol.* **36,** 891–931.

Rapp R. P., Shimizu N., Norman M. D., and Applegate G. S. (1999) Reaction between slab-derived melts and peridotite in the mantle wedge: Experimental constraints at 3.8 GPa. *Chem. Geol.* **160,** 335–356.

Rapp R. P., Shimizu N., and Norman M. D. (2003) Growth of early continental crust by partial melting of eclogite. *Nature* **425,** 605–609.

Righter K., Hill D., Collins J., Capobianco C. J., and Drake M. J. (2001) Experimental studies of metal-silicate partitioning of Sb. *Meteoritics and Planetary Sciences* **36** Suppl. A 5401.

Rudnick R. L., Barth M., Horn I., and McDonough W. F. (2000) Rutile-bearing refractory eclogites: Missing link between continents and depleted mantle. *Science* **287,** 278–281.

Ryan J. G., Morris J., Tera F., Leeman W. P., and Tsvetkov A. (1995) Cross-arc geochemical variations in the Kurile Arc as a function of slab depth. *Science* **270,** 625–627.

Ryerson F. J. and Hess P. C. (1978) Implications of liquid-liquid distribution coefficients to mineral-liquid partitioning. *Geochim. Cosmochim. Acta* **42,** 921–932.

Ryerson F. J. and Watson E. B. (1987) Rutile saturation in magmas: Implications for Ti-Nb-Ta depletion in island-arc basalts. *Earth Planet. Sci. Lett.* **86,** 225–239.

Schmid G., Witt-Eicksen G., Palme H., Seck H., Spettel B., and Kratz K.-L. (2003) Highly siderophile elements (PGE, Re and Au) in mantle xenoliths from the West Eifel volcanic field, Germany. *Chem. Geol.* **196,** 77–105.

Schmidt M. W., Dardon A., Chazot G., and Vannucci R. (2004) The dependence of Nb and Ta rutile-melt partitioning on melt composition and Nb/Ta fractionation during subduction processes. *Earth Planet. Sci. Lett.,* **226,** 415–432.

Shannon R. D. (1976) Revised effective ionic radii and systematic studies of interatomic distances in halides and chalcogenides. *Acta Cryst.* **32,** 751–767.

Sigmarsson O., Martin H., and Knowles J. (1998) Melting of subducting oceanic crust from U-Th disequilibria in Austral Andean lavas. *Nature* **394,** 566–569.

Stalder R., Foley S. F., Brey G. P., and Horn I. (1998) Mineral aqueous fluid partitioning of trace elements at 900–1200 degrees C and 3.0–5.7 GPa: New experimental data for garnet, clinopyroxene, and rutile and implications for mantle metasomatism. *Geochim. Cosmochim. Acta* **62,** 1781–1801.

Stern C. R. and Kilian R. (1996) Role of the subducted slab, mantle wedge and continental crust in the generation of adakites from the Andean Austral Volcanic Zone. *Contrib. Mineral. Petrol.* **123,** 263–281.

Tatsumi Y. and Eggins S. (1995) *Subduction Zone Magmatism.* Blackwell Science.

Tiepolo M., Vannucci R., Oberti R., Foley S., Bottazzi P., and Zanetti A. (2000) Nb and Ta incorporation and fractionation in titanian pargasite and kaersutite: Crystal-chemical constraints and implications for natural systems. *Earth Planet. Sci. Lett.* **176,** 185–201.

Turner S. T., Hawkesworth C., van Calsteren P., Health E., Macdonald R., and Black S. (1996) U-series isotopes and destructive margin magma genesis in the Lesser Antilles. *Earth Planet. Sci. Lett.* **142,** 191–207.

Turner S., McDermott F., Hawkesworth C. J., and Kepezhinskas P. (1998) A U-series study of lavas from Kamchatka and the Aleutians: Constraints on source composition and melting process. *Contrib. Mineral. Petrol.* **133,** 217–234.

Turner S., Bourdon B., Hwakesworth C. J., and Evans P. (2000) ^{226}Ra-^{230}Th evidence for multiple dehydration events, rapid melt ascent and time scales for differentiation beneath the Tongo-Kermadec island arc. *Earth Planet. Sci. Lett.* **179,** 581–593.

Turner S., Evans P., and Hawkesworth C. J. (2001) Ultrafast-source to surface movement of melt at island arcs from ^{226}Ra-^{230}Th systematics. *Science* **292,** 1363–1366.

Watson E. B. (1976) Two liquid partition-coefficients—Experimental data and geochemical implications. *Contrib. Mineral. Petrol.* **56,** 119–134.

Yogodzinski G. M. and Kelemen P. B. (1998) Slab melting in the Aleutians: Implications of an ion probe study of clinopyroxene in primitive adakite and basalt. *Earth Planet. Sci. Lett.* **158,** 53–65.

Zack T., Kronz A., Foley S. F., and Rivers T. (2002) Trace element abundances in rutiles from eclogites and associated garnet mica schists. *Chem. Geol.* **184,** 97–122.

Zack T., Moraes R., and Kronz A. (2004) Temperature-dependence of Zr in rutile: Empirical calibration of a rutile thermometer. *Contrib. Mineral. Petrol.,* **148,** 471–488.

Zhang R. Y., Zhai S. M., Fei Y. W., and Liou J. G. (2003) Titanium solubility in coexisting garnet and clinopyroxene at very high pressure: The significance of exsolved rutile in garnet. *Earth Planet. Sci. Lett.* **216,** 591–601.

Zhao G. C., Cawood P., and Lu L. Z. (1999) Petrology and P-T history of the Wutai amphibolites: Implications for tectonic evolution of the Wutai Complex, China. *Precam. Res.* **93,** 181–199.